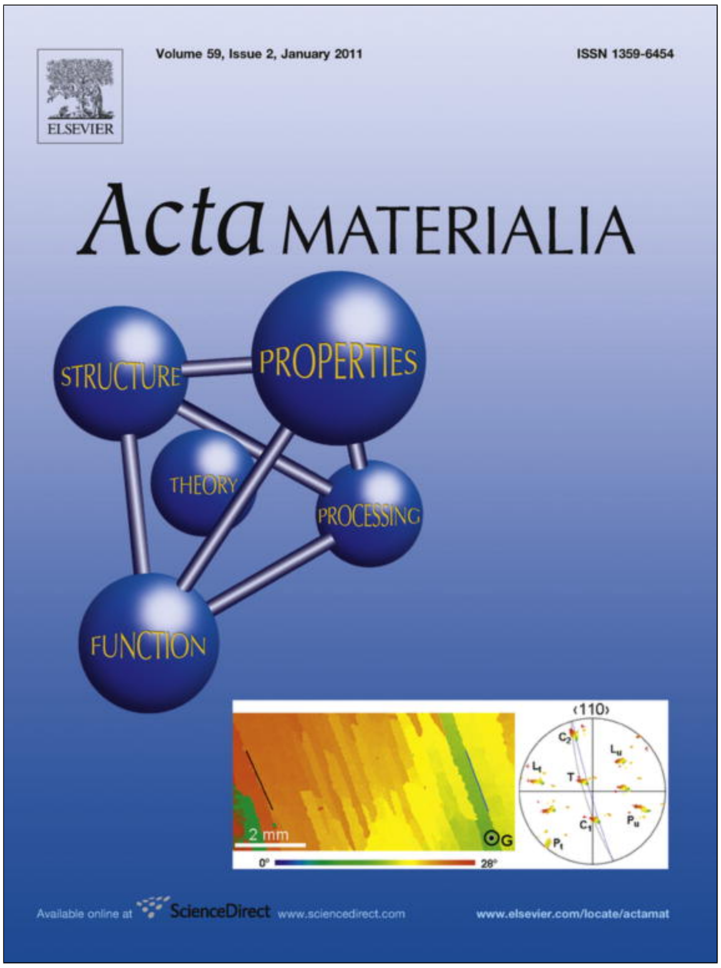
Volume 59, Issue 2, January 2011
ISSN 1359-6454
ELSEVIER
Acta MATERIALIA
STRUCTURE
PROPERTIES
THEORY
PROCESSING
FUNCTION
2 mm
Available online at ScienceDirect www.sciencedirect.com
www.elsevier.com/locate/actamat

ELSEVIER

Available online at www.sciencedirect.com

ScienceDirect

Acta Materialia 59 (2011) 797–804

Acta MATERIALIA

www.elsevier.com/locate/actamat

Interaction between an edge dislocation and a circular inclusion with interface slip and diffusion

Xu Wang [a], Ernie Pan [a,b,*]

[a] School of Mechanical Engineering, Zhengzhou University, Zhengzhou, Henan 450001, People's Republic of China
[b] Department of Civil Engineering, University of Akron, OH 44325, USA

Received 1 July 2010; received in revised form 8 October 2010; accepted 9 October 2010
Available online 31 October 2010

Abstract

We investigate in detail the transient response induced by an edge dislocation near a circular elastic inclusion with simultaneous interface slip and diffusion. A rigorous solution to the interaction problem is derived in series form. As the time approaches infinity, our solution just recovers the classical one derived by Srolovitz et al. (Acta Metall 1984;32:1079) for fully relaxed boundary conditions. In addition, we observe that the edge dislocation will induce a uniform rigid-body rotation in the inclusion as the time approaches infinity. When the dislocation is far away from the inclusion, simple asymptotic expressions of the glide and climb forces on the dislocation are also obtained. Furthermore, five extreme cases for the imperfect interface are discussed; in particular, we derive approximate closed-form expressions of the decaying internal stress field within the inclusion and the image force on the dislocation for long-range stress relaxations when the interface diffusion occurs much faster than the interface slip and vice versa. Some interesting physical behaviors are observed.

Keywords: Edge dislocation; Interface diffusion; Interface slip; Relaxation times; Image force

1. Introduction

Interface slip, which leads to viscous-like relaxation of the shear traction, is due to diffusion over length scales comparable to the size of the asperities of the interface [1]; whilst interface diffusion, which causes relaxation of the normal traction gradient along the interface, is driven by the gradient of chemical potential on the interface [2,3]. Interface slip and diffusion should be taken into consideration when discussing the dislocation–inclusion interaction at elevated temperatures [4–8]. Srolovitz et al. [7] were the first to derive an exact solution for the elastic problem of an edge dislocation interacting with a circular inclusion assuming that both the tangential traction and normal traction gradients are instantaneously relaxed at the inclusion/matrix interface. A recent summary of historical developments in the understanding of the dislocation–particle interaction at elevated temperature can be found in Ref. [9].

Srolovitz et al.'s solution [7] is valid for the steady-state creep in which both the interface slip and diffusion relaxation processes have finished as the time approaches infinity. As observed in Ref. [10], some important phenomena may only occur in a transient period of time and would disappear at steady state. Thus the main purpose of this work is to investigate the transient response caused by an edge dislocation interacting with a circular inclusion with interface slip and diffusion. This paper is structured as follows. In Section 2, we derive the time-dependent elastic field caused by an edge dislocation near a circular inclusion by means of the complex variable method. The time-dependent image force acting on the dislocation is obtained in Section 3. Five extreme cases of the imperfect interface are discussed in Section 4, with detailed numerical results to show the mobility of the dislocation due to its interaction with the inclusion. Finally, conclusions are drawn in Section 5.

* Corresponding author at: Department of Civil Engineering, University of Akron, OH 44325, USA.
E-mail address: pan2@uakron.edu (E. Pan).

1359-6454/$36.00 © 2010 Acta Materialia Inc. Published by Elsevier Ltd. All rights reserved.
doi:10.1016/j.actamat.2010.10.024

2. Time-dependent elastic field

Here we consider a solitary circular elastic inclusion of radius R bonded to an infinite matrix through a sharp interface L, as illustrated in Fig. 1. We establish a Cartesian coordinate system xoy, with its origin at the center of the circular inclusion. Furthermore, we assume that an edge dislocation with Burgers vector (b_x, b_y) is introduced at the initial time and is fixed at $(\xi, 0)$ on the x-axis in the matrix. In the following analysis, all physical quantities pertaining to the inclusion and matrix will be labeled with subscripts 1 and 2 (or superscripts (1) and (2)), respectively.

For the in-plane deformation of an isotropic elastic material, the stresses, displacements and resultant forces can be expressed in terms of two analytic functions $\phi(z, t)$ and $\psi(z, t)$ as [11]

$$\begin{aligned} &\sigma_{rr}+\sigma_{\theta\theta} = 2\left[\phi'(z,t)+\overline{\phi'(z,t)}\right],\\ &\sigma_{rr}-\mathrm{i}\sigma_{r\theta} = \phi'(z,t)+\overline{\phi'(z,t)}-e^{2\mathrm{i}\theta}[\bar{z}\phi''(z,t)+\psi'(z,t)],\\ &2\mu(u_r+\mathrm{i}u_\theta) = e^{-\mathrm{i}\theta}\left[\kappa\phi(z,t)-z\overline{\phi'(z,t)}-\overline{\psi(z,t)}\right],\\ &X+\mathrm{i}Y = -\mathrm{i}\left[\phi(z,t)+z\overline{\phi'(z,t)}+\overline{\psi(z,t)}\right], \end{aligned} \tag{1}$$

where $\kappa = 3-4\nu$ is for plane-strain deformation, which is assumed in this investigation, and $\kappa = (3-\nu)/(1+\nu)$ for plane-stress deformation; μ and ν, where $\mu > 0$ and $0 \leqslant \nu \leqslant 0.5$, are the shear modulus and Poisson's ratio, respectively; t is the real time variable; and $z = x+\mathrm{i}y = re^{\mathrm{i}\theta}$ is the complex variable. The appearance of the real time in the above expression is solely due to the rate-dependent interface slip and diffusion on L. The interface slip and diffusion boundary conditions can be expressed as [1–3,10,12]

$$\begin{aligned} &\sigma_{r\theta}^{(1)} = \sigma_{r\theta}^{(2)} = \eta\left(\dot{u}_\theta^{(2)}-\dot{u}_\theta^{(1)}\right),\\ &\qquad \frac{D}{R^2}\frac{\mathrm{d}^2\sigma_{rr}^{(1)}}{\mathrm{d}\theta^2} = \frac{D}{R^2}\frac{\mathrm{d}^2\sigma_{rr}^{(2)}}{\mathrm{d}\theta^2} = \dot{u}_r^{(1)}-\dot{u}_r^{(2)}, \text{ on } L \end{aligned} \tag{2}$$

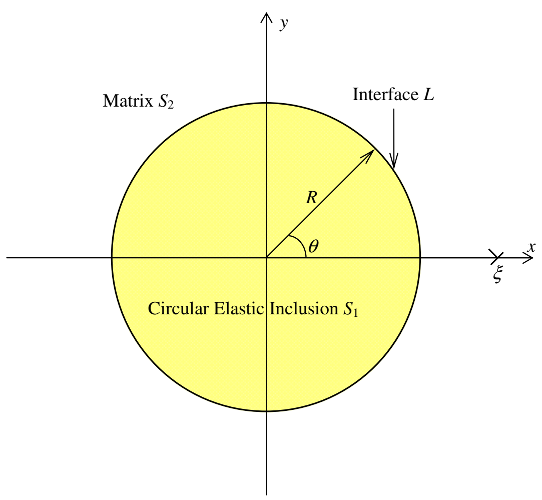

Fig. 1. An edge dislocation near a circular inclusion embedded in a matrix.

where the overdot denotes the derivative with respect to time t, η is a non-negative interface drag parameter and D is a non-negative interface diffusion parameter. Here we assume that both η and D are constant along the circular interface.

If we introduce the following analytic continuations

$$\phi_i(z,t) = -z\bar{\phi}_i'(R^2/z,t)-\bar{\psi}_i(R^2/z,t), \quad i=1,2 \tag{3}$$

then it can be strictly proved that $\phi_1'(0,t)$ is, in fact, time-independent (hence in the following we can write $\phi_1'(0,t)=\phi_1'(0)$), and that $\phi_1(z,t)$ should satisfy the following set of partial differential equations [13]

$$\begin{aligned} &\dot{\phi}_1(z,t)-\alpha\frac{z^2}{R^2}\dot{\bar{\phi}}_1(R^2/z,t)\\ &\quad+\frac{1}{\chi}z\left[\phi_1'(z,t)+\bar{\phi}_1'(R^2/z,t)\right]=0, \quad (|z|<R) \end{aligned} \tag{4}$$

$$\begin{aligned} &\alpha\dot{\phi}_1(z,t)-\frac{z^2}{R^2}\dot{\bar{\phi}}_1(R^2/z,t)\\ &\quad-\frac{1}{\chi}z\left[\phi_1'(z,t)+\bar{\phi}_1'(R^2/z,t)\right]=0, \quad (|z|>R) \end{aligned} \tag{5}$$

$$\begin{aligned} &\dot{\phi}_1(z,t)+\alpha\frac{z^2}{R^2}\dot{\bar{\phi}}_1(R^2/z,t)\\ &\quad+\frac{1}{4\gamma}\left[z^2\phi_1''(z,t)+z^3\phi_1'''(z,t)-R^2\bar{\phi}_1''(R^2/z,t)-\frac{R^4}{z}\bar{\phi}_1'''(R^2/z,t)\right]\\ &\quad=0, \quad (|z|<R) \end{aligned} \tag{6}$$

$$\begin{aligned} &\alpha\dot{\phi}_1(z,t)+\frac{z^2}{R^2}\dot{\bar{\phi}}_1(R^2/z,t)\\ &\quad-\frac{1}{4\gamma}\left[z^2\phi_1''(z,t)+z^3\phi_1'''(z,t)-R^2\bar{\phi}_1''(R^2/z,t)-\frac{R^4}{z}\bar{\phi}_1'''(R^2/z,t)\right]\\ &\quad=0, \quad (|z|>R) \end{aligned} \tag{7}$$

where α and β are two dimensionless parameters defined by

$$\alpha = \frac{\kappa_2\mu_1+\mu_2}{\kappa_1\mu_2+\mu_1}, \quad \beta = \frac{\kappa_2\mu_1+\mu_1}{\kappa_1\mu_2+\mu_1}, \tag{8}$$

and χ and γ are two time scales (corresponding to the interface slip and diffusion) defined by

$$\chi = \frac{\eta R(\kappa_1\mu_2+\mu_1)}{2\mu_1\mu_2}, \quad \gamma = \frac{R^3(\kappa_1\mu_2+\mu_1)}{8\mu_1\mu_2 D} \tag{9}$$

The analytic function $\phi_1(z,t)$ in its original region $|z|<R$ and in its continuation region $|z|>R$ can then be expanded into the following forms:

$$\begin{aligned} &\phi_1(z,t) = \phi_1'(0)z+\sum_{n=2}^{+\infty}A_n(t)z^n, \quad (|z|<R)\\ &\phi_1(z,t) = -\overline{\phi_1'(0)}z+\sum_{n=3}^{+\infty}R^{2(n-1)}\overline{B_n(t)}z^{-(n-2)}, \quad (|z|>R) \end{aligned} \tag{10}$$

where $A_n(t)$ and $B_n(t)$ are time-dependent parameters to be determined.

Substituting the above expressions into Eqs. (4)–(7), we arrive at

$$A_2(t)=A_2(0)\exp\left(-\frac{t}{t_0}\right), \tag{11}$$

$$\begin{aligned}A_n(t)&=P_n\left[\chi\alpha-(n-2)t_n^-\right]\exp\left(-\frac{t}{t_n^-}\right)\\&\quad+Q_n\left[\chi\alpha-(n-2)t_n^+\right]\exp\left(-\frac{t}{t_n^+}\right),\\B_n(t)&=P_n\left(\chi-nt_n^-\right)\exp\left(-\frac{t}{t_n^-}\right)\\&\quad+Q_n\left(\chi-nt_n^+\right)\exp\left(-\frac{t}{t_n^+}\right),(n=3,4,\ldots,+\infty)\end{aligned} \tag{12}$$

where t_0 and t_n^-, t_n^+ $(n = 3, 4, \ldots, +\infty)$ are the relaxation times given by

$$t_0=\frac{4\chi\gamma}{\chi+4\gamma}\geqslant 0, \tag{13}$$

$$\begin{aligned}t_n^-&=\frac{[n(\alpha+1)-2][4\gamma+\chi(n-1)^2]-\sqrt{[n(\alpha+1)-2]^2[4\gamma+\chi(n-1)^2]^2-64\alpha\chi\gamma n(n-2)(n-1)^2}}{4n(n-2)(n-1)^2}\geqslant 0,\\t_n^+&=\frac{[n(\alpha+1)-2][4\gamma+\chi(n-1)^2]+\sqrt{[n(\alpha+1)-2]^2[4\gamma+\chi(n-1)^2]^2-64\alpha\chi\gamma n(n-2)(n-1)^2}}{4n(n-2)(n-1)^2}\geqslant 0,(n=3,4,\ldots,+\infty)\end{aligned} \tag{14}$$

and the constants P_n and Q_n are related to $A_n(0)$ and $B_n(0)$ through the following expressions

$$\begin{aligned}P_n&=\frac{(\chi-nt_n^+)A_n(0)+[(n-2)t_n^+-\chi\alpha]B_n(0)}{(\chi-nt_n^+)[\chi\alpha-(n-2)t_n^-]-(\chi-nt_n^-)[\chi\alpha-(n-2)t_n^+]},\\Q_n&=\frac{(\chi-nt_n^-)A_n(0)+[(n-2)t_n^--\chi\alpha]B_n(0)}{(\chi-nt_n^-)[\chi\alpha-(n-2)t_n^+]-(\chi-nt_n^+)[\chi\alpha-(n-2)t_n^-]}\\&(n=3,4,\ldots,+\infty)\end{aligned} \tag{15}$$

It is clearly observed from the above derivations that: (i) $A_2(t)$ decays with one single relaxation time t_0; and (ii) $A_n(t)$ and $B_n(t)$ $(n \geqslant 3)$ decay with two different relaxation times, t_n^- and t_n^+. Thus the internal stresses inside the inclusion will decay with all the relaxation times t_0, t_n^- and t_n^+ $(n = 3, 4, \ldots, +\infty)$.

In view of the fact that the interface is perfect at the initial moment, we then have

$$\phi_1'(0)=\frac{\beta\mu_2}{\pi\xi(\kappa_2+1)}\left(\frac{b_y}{\alpha-\beta-1}+\frac{\mathrm{i}b_x}{\alpha-\beta+1}\right), \tag{16}$$

and

$$\begin{aligned}A_n(0)&=-\frac{\beta\xi^{-n}A}{n},(n=2,3,\ldots,+\infty)\\B_n(0)&=\frac{\beta}{\alpha}\left[\frac{\xi^{-(n-2)}\bar{A}}{R^2(n-2)}+\xi^{-n}(1-\xi^2R^{-2})A\right],\\&(n=3,4,\ldots,+\infty)\end{aligned} \tag{17}$$

where

$$A=\frac{\mu_2(b_x+\mathrm{i}b_y)}{\pi\mathrm{i}(\kappa_2+1)} \tag{18}$$

The analytic function $\phi_2(z,t)$ in its original region $|z| > R$ and in its continuation region $|z| < R$ can then be easily obtained as

$$\begin{aligned}\phi_2(z,t)&=-2\mathrm{Re}\{\phi_1'(0)\}z+A\ln(z-\xi)-A\ln\frac{z-R^2/\xi}{z}\\&\quad+\frac{R^2(R^2-\xi^2)}{\xi^3}\frac{\bar{A}}{z-R^2/\xi}-\sum_{n=2}^{+\infty}A_n(t)z^n,\quad(|z|<R)\\\phi_2(z,t)&=A\ln(z-\xi)-A\ln\frac{z-R^2/\xi}{z}+\frac{R^2(R^2-\xi^2)}{\xi^3}\frac{\bar{A}}{z-R^2/\xi}\\&\quad-\sum_{n=3}^{+\infty}R^{2(n-1)}\overline{B_n(t)}z^{-(n-2)},\quad(|z|>R)\end{aligned} \tag{19}$$

As time t approaches infinity, the two analytic functions within the inclusion become

$$\phi_1(z,\infty)=\phi_1'(0)z,\psi_1(z,\infty)=0\quad(|z|<R) \tag{20}$$

which indicates that the internal stresses are uniform and hydrostatic such that

$$\begin{aligned}\sigma_{xx}=\sigma_{yy}&=\frac{2\beta\mu_2b_y}{\pi\xi(\kappa_2+1)(\alpha-\beta-1)}=\frac{\mu_1\mu_2b_y}{\pi\xi[(2\nu_1-1)\mu_2-\mu_1]},\\\sigma_{xy}&=0,t\to\infty,\quad(|z|<R)\end{aligned} \tag{21}$$

Furthermore, as time t approaches infinity, the edge dislocation will induce the following uniform rigid-body rotation in the inclusion

$$\varepsilon=\frac{\beta\mu_2(\kappa_1+1)b_x}{2\pi\xi\mu_1(\kappa_2+1)(\alpha-\beta+1)}=\frac{b_x}{2\pi\xi}. \tag{22}$$

It can be easily checked that Eq. (21) is in agreement with the result obtained by Srolovitz et al. [7] using Eshelby's method. In addition, it is of interest to note that the induced uniform rigid-body rotation in the inclusion is independent of the material properties of both the inclusion and the matrix, and is also independent of the size of the inclusion.

3. Time-dependent force on the dislocation

By employing the Peach–Koehler formula [14], we can obtain the time-dependent image force acting on the edge dislocation due to its interaction with the circular inclusion.

The specific expression of the image force is rather lengthy and is suppressed here. However, if the dislocation is far from the inclusion and contains only the b_x component, then the glide force F_x can be simply approximated as

$$F_x = \frac{4\mu_2 R^2 (b_x)^2}{\pi\xi^3(\kappa_2+1)} \times \left[\frac{\beta\left[(\chi-3t_3^+)(\chi\alpha-t_3^-)\exp(-\frac{t}{t_3^+})-(\chi-3t_3^-)(\chi\alpha-t_3^+)\exp(-\frac{t}{t_3^-})\right]}{\chi\alpha(3\alpha-1)(t_3^- - t_3^+)} - 1\right] + o(\xi^{-5}), \text{ as } |\xi| \gg R \text{ and } t \geqslant 0 \tag{23}$$

which will reduce to Dundurs and Mura's result [15] when $t = 0$. The above far-field asymptotic expression indicates that, in general, the glide force evolves with two relaxation times, t_3^- and t_3^+. It is also of interest to note that, except for the pre-factor, the above expression is similar in form to that of the effective in-plane shear modulus for a material containing a dilute and random dispersion of the same circular inclusions with interface slip and diffusion [13].

Similarly, if the dislocation is far from the inclusion and contains only the b_y component, then the climb force F_x can be simply approximated as

$$F_x = \frac{2\mu_2 R^2 (b_y)^2}{\pi\xi^3(\kappa_2+1)} \frac{\alpha-1}{1-\alpha+\beta} + o(\xi^{-5}), \text{ as } |\xi| \gg R \text{ and } t \geqslant 0 \tag{24}$$

which is the same result obtained by Dundurs and Mura [15]. Eq. (24) indicates that the interface slip and diffusion exert no influence on the far-field asymptotic climb force.

4. Discussion of extreme cases of the interface

In this section, we investigate the physical behavior of the dislocation–inclusion interaction problem by considering five extreme cases of the interface: (i) the interface diffusion is absent (or a pure slip interface); (ii) the interface slip is absent (or a pure diffusion interface); (iii) the interface slip occurs much faster than the interface diffusion; (iv) the interface diffusion occurs much faster than the interface slip; and (v) the interface diffusion and slip have the same time scale, $\chi = \gamma$.

4.1. The interface diffusion is absent ($\gamma \to \infty$)

In this case, the relaxation times can be determined from Eqs. (13) and (14) as

$$t_0 = \chi, \; t_n^- = \frac{2\alpha\chi}{n(\alpha+1)-2}, \quad t_n^+ \to \infty, \quad (n = 3, 4, \ldots, +\infty) \tag{25}$$

where $t_0 > t_n^-$. $A_n(t)$ and $B_n(t)$ can be explicitly determined as

$$A_n(t) = \frac{\alpha[nA_n(0)-(n-2)B_n(0)]}{n(\alpha+1)-2}\exp\left(-\frac{t}{t_n^-}\right) + \frac{(n-2)[A_n(0)+\alpha B_n(0)]}{n(\alpha+1)-2},$$

$$B_n(t) = \frac{(n-2)B_n(0)-nA_n(0)}{n(\alpha+1)-2}\exp\left(-\frac{t}{t_n^-}\right) + \frac{n[A_n(0)+\alpha B_n(0)]}{n(\alpha+1)-2}, (n = 3, 4, \ldots, +\infty) \tag{26}$$

If the dislocation is far from the inclusion and contains only the b_x component, then the glide force F_x can be obtained from Eq. (23) as

$$F_x = \frac{4\mu_2 R^2 (b_x)^2}{\pi\xi^3(\kappa_2+1)(3\alpha+1)}\left[3(\beta-\alpha)-1+\frac{\beta}{\alpha}\exp(-\frac{t}{t_3^-})\right], \text{ as } |\xi| \gg R \text{ and } t \geqslant 0 \tag{27}$$

which reduces to the result by Dundurs and Gangadharan [16] when $t \to \infty$. Furthermore, if $\beta - \alpha > 1/3$ (or equivalently $\mu_1/\mu_2 > 3 - 2\nu_1$), the dislocation will always be repelled from the inclusion at any time. On the other hand, if $0 < \beta - \alpha < 1/3$ (or equivalently $1 < \mu_1/\mu_2 < 3 - 2\nu_1$), the dislocation will be attracted to or repelled from the inclusion depending on the time: (i) the dislocation will be repelled from the inclusion when $t < t_3^- \ln\left(\frac{\beta}{\alpha[3(\alpha-\beta)+1]}\right)$; (ii) the dislocation will be attracted to the inclusion when $t > t_3^- \ln\left(\frac{\beta}{\alpha[3(\alpha-\beta)+1]}\right)$.

4.2. The interface slip is absent ($\chi \to \infty$)

In this case, the relaxation times can be determined from Eqs. (13) and (14) as

$$t_0 = 4\gamma, \; t_n^- = \frac{8\alpha\gamma}{(n-1)^2[n(\alpha+1)-2]}, \quad t_n^+ \to \infty, \quad (n = 3, 4, \ldots, +\infty) \tag{28}$$

$A_n(t)$ and $B_n(t)$ can be explicitly determined as

$$A_n(t) = \frac{\alpha[nA_n(0)+(n-2)B_n(0)]}{n(\alpha+1)-2}\exp\left(-\frac{t}{t_n^-}\right) + \frac{(n-2)[A_n(0)-\alpha B_n(0)]}{n(\alpha+1)-2},$$
$$B_n(t) = \frac{(n-2)B_n(0)+nA_n(0)}{n(\alpha+1)-2}\exp\left(-\frac{t}{t_n^-}\right) + \frac{n[\alpha B_n(0)-A_n(0)]}{n(\alpha+1)-2}, (n = 3, 4, \ldots, +\infty) \tag{29}$$

If the dislocation is far from the inclusion and contains only the b_x component, then the glide force F_x can be obtained from Eq. (23) as

$$F_x = \frac{4\mu_2 R^2 (b_x)^2}{\pi\xi^3(\kappa_2+1)(3\alpha+1)}\left[3(\beta-\alpha)-1+\frac{\beta}{\alpha}\exp\left(-\frac{t}{t_3^-}\right)\right]. \tag{30}$$

Interestingly, the above expression is very similar to Eq. (27) except that the definitions of t_3^- for the two cases are different. Therefore, the dislocation behavior, i.e. whether the dislocation is attracted to or repelled from the inclusion, is the same as that in Section 4.1.

4.3. The interface slip occurs much faster than the interface diffusion ($\chi \to 0$)

This kind of interface, on which the shear traction is fully relaxed (i.e. $\sigma_{r\theta} = 0$), is the one discussed by Koeller and Raj [3]. In this case, the relaxation times can be determined from Eqs. (13) and (14) as

$$t_0 = t_n^- = 0, t_n^+ = \frac{2\gamma[n(\alpha+1)-2]}{n(n-2)(n-1)^2} = \frac{2\gamma}{(n-1)^2}\left[\frac{\alpha}{n-2}+\frac{1}{n}\right], \quad (n = 3, 4, \ldots, +\infty) \tag{31}$$

$A_n(t)$ and $B_n(t)$ can be determined as

$$A_2(t) = 0,$$
$$A_n(t) = \frac{(n-2)[A_n(0)+\alpha B_n(0)]}{n(\alpha+1)-2}\exp\left(-\frac{t}{t_n^+}\right), \quad (n = 3, 4, \ldots, +\infty) \tag{32}$$
$$B_n(t) = \frac{n[A_n(0)+\alpha B_n(0)]}{n(\alpha+1)-2}\exp\left(-\frac{t}{t_n^+}\right),$$

It is found that $t_3^+ = \gamma(3\alpha+1)/6$ is the longest time constant among all the relaxation times $t_n^+ (n \geqslant 3)$. Thus for the long-range stress relaxations one needs only to retain the terms $A_3(t)$ and $B_3(t)$ in the series expansions in Eqs. (10) and (19). The decaying internal stress field for long-range stress relaxations can thus be approximated as

$$\sigma_{xx} = \frac{2\beta\mu_2 b_y}{\pi\xi(\kappa_2+1)(\alpha-\beta-1)} + \frac{4\beta\mu_2[R^2(-2y^2+R^2)b_y - 2xy(3\xi^2-R^2)b_x]}{\pi R^2\xi^3(\kappa_2+1)(3\alpha+1)}\exp\left(-\frac{t}{t_3^+}\right)$$
$$\sigma_{yy} = \frac{2\beta\mu_2 b_y}{\pi\xi(\kappa_2+1)(\alpha-\beta-1)} + \frac{4\beta\mu_2[R^2(2x^2-R^2)b_y - 2xy(3\xi^2-R^2)b_x]}{\pi R^2\xi^3(\kappa_2+1)(3\alpha+1)}\exp\left(-\frac{t}{t_3^+}\right),$$
$$\sigma_{xy} = \frac{4\beta\mu_2(3\xi^2-R^2)(x^2+y^2-R^2)b_x}{\pi R^2\xi^3(\kappa_2+1)(3\alpha+1)}\exp\left(-\frac{t}{t_3^+}\right), (x^2+y^2<R^2) \tag{33}$$

By employing the Peach–Koehler formula, we arrive at an approximate closed-form expression of the image force on the dislocation for long-range stress relaxations as

$$F_x = F_x^0 + \frac{2\beta\mu_2 R^2(b_y)^2}{\pi\xi^3(\kappa_2+1)(1-\alpha+\beta)} + \frac{4\beta\mu_2 R^2[(\xi^2-R^2)(3\xi^2-R^2)(b_x)^2 + R^4(b_y)^2]}{\pi\xi^7(\kappa_2+1)(3\alpha+1)}\exp\left(-\frac{t}{t_3^+}\right),$$
$$F_y = F_y^0 + \frac{2\beta\mu_2 R^2 b_x b_y}{\pi\xi^3(\kappa_2+1)(1-\alpha+\beta)} - \frac{4\beta\mu_2 R^2(3\xi^2-2R^2)b_x b_y}{\pi\xi^5(\kappa_2+1)(3\alpha+1)}\exp\left(-\frac{t}{t_3^+}\right), |\xi| > R \tag{34}$$

where F_x and F_y are, respectively, the x- and y-components of the image force, and F_x^0 and F_y^0 correspond to the image force for the edge dislocation near a circular hole [7].

If the dislocation is far from the inclusion and contains only the b_x component, then the glide force F_x can be obtained from Eq. (23) as

$$F_x = \frac{4\mu_2 R^2(b_x)^2}{\pi\xi^3(\kappa_2+1)}\left[\frac{3\beta}{3\alpha+1}\exp\left(-\frac{t}{t_3^+}\right) - 1\right], \text{ as } |\xi| \gg R \text{ and } t \geqslant 0 \tag{35}$$

which reduces to the result by Dundurs and Gangadharan [16] when $t = 0$. Furthermore, if $\beta - \alpha < 1/3$ (or equivalently $\mu_1/\mu_2 < 3 - 2\nu_1$), the dislocation will always be attracted to the inclusion. On the other hand, if $\beta - \alpha > 1/3$ (or equivalently $\mu_1/\mu_2 > 3 - 2\nu_1$), the dislocation will be attracted to or repelled from the inclusion depending on the time: (i) the dislocation will be repelled from the inclusion when $t < t_3^+ \ln(\frac{3\beta}{3\alpha+1})$; (ii) the dislocation will be attracted to the inclusion when $t > t_3^+ \ln(\frac{3\beta}{3\alpha+1})$.

In order to show the dislocation mobility due to its interaction with the inclusion more clearly, we illustrate in Fig. 2 the time-dependent glide force F_x on a dislocation containing only the b_x component for $\mu_1 = 10\mu_2$ and $\nu_1 = \nu_2 = 1/3$ by using the following exact solution:

$$F_x = \frac{\mu_2(b_x)^2}{\pi(\kappa_2+1)}\left[-\frac{2R^2(2\xi^2-R^2)}{\xi^3(\xi^2-R^2)} + \beta(\xi^2-R^2) \times \sum_{n=3}^{+\infty}\frac{(n-1)^2R^{2(n-2)}[n\xi^2-(n-2)R^2]}{\xi^{2n+1}[n(\alpha+1)-2]} \times \exp\left(-\frac{t}{t_n^+}\right)\right]. \ |\xi| > R \text{ and } t \geqslant 0 \tag{36}$$

It is strictly proved that, when $t = 0$, the above expression is equivalent to Eq. (15) in Dundurs and Gangadharan [16]. In calculating the curves in Fig. 2 (and also in Figs. 3 and 4 below), the series in Eq. (36) is truncated at $n = 50$ to obtain results with relative errors less than 0.01%. It is observed from Fig. 2 that when $0 < t < 0.2128t_3^+$ the dislocation has a transient unstable equilibrium position at $\xi = \xi_0$. This means that at this moment the dislocation will be attracted to the inclusion if $\xi < \xi_0$ and be repelled from the inclusion if $\xi > \xi_0$. Furthermore, the equilibrium position will move outward from $\xi = R$ to infinity as the time increases from $t = 0^+$ to $t = 0.2128t_3^+$ (see Table 1). On the other hand, when $t > 0.2128t_3^+$, the dislocation will always be attracted to the inclusion. Our calculations also

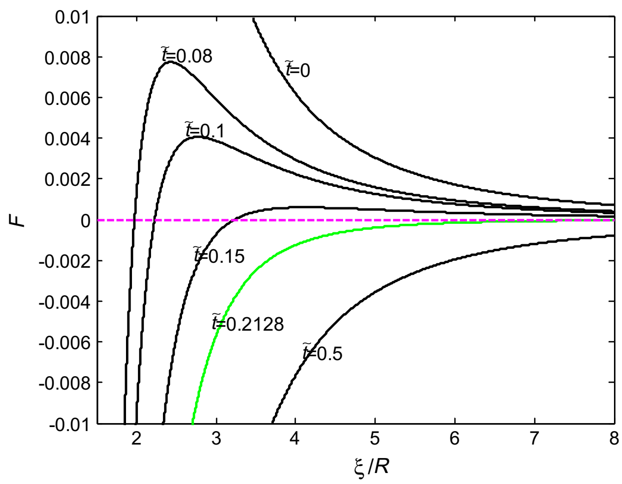

Fig. 2. The normalized glide force $F = \frac{\pi R F_x}{\mu_2(b_x)^2}$ on a dislocation containing only the b_x component at six moments, $\tilde{t} = t/t_3^+ = 0, 0.08, 0.1, 0.15, 0.2128, 0.5$. $\mu_1 = 10\mu_2$ and $\nu_1 = \nu_2 = 1/3$ (these material parameters satisfy $\mu_1/\mu_2 > 3 - 2\nu_1$), $\chi \to 0$.

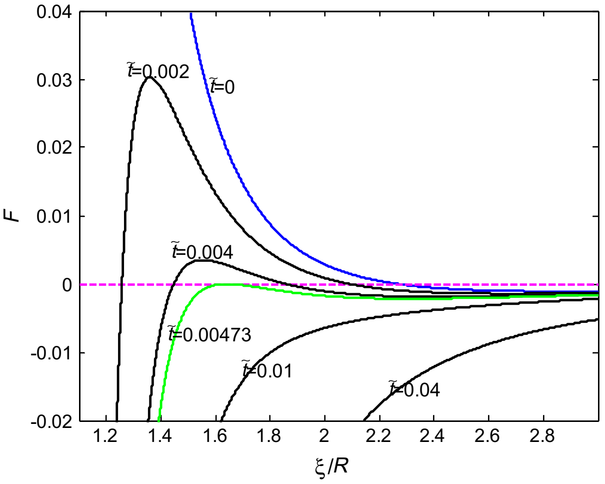

Fig. 3. The normalized glide force $F = \frac{\pi R F_x}{\mu_2 \langle b_x \rangle^2}$ on a dislocation containing only the b_x component at six moments, $\tilde{t} = t/t_3^+ = 0, 0.002, 0.004, 0.00473, 0.01, 0.04$, under the conditions $\chi \to 0$, $\mu_1 = 2\mu_2$ and $v_1 = v_2 = 1/3$ (these material parameters satisfy $1 < \mu_1/\mu_2 < 3 - 2v_1$).

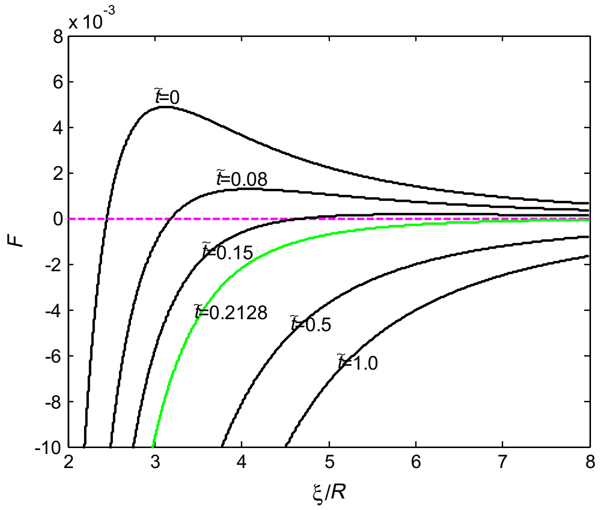

Fig. 4. The normalized glide force $F = \frac{\pi R F_x}{\mu_2 \langle b_x \rangle^2}$ on a dislocation containing only the b_x component at six moments, $\tilde{t} = t/t_3^+ = 0, 0.08, 0.15, 0.2128, 0.5, 1.0$, under the conditions $\gamma \to 0$, $\mu_1 = 10\mu_2$ and $v_1 = v_2 = 1/3$ (these material parameters satisfy $\mu_1/\mu_2 > 3 - 2v_1$).

indicate that, for $t \geqslant 0.5t_3^+$, the approximate expression (34) for the long-range stress relaxations can be used with very high accuracy.

Fig. 3 presents the time-dependent glide force F_x on a dislocation containing only the b_x component for $\mu_1 = 2\mu_2$ and $v_1 = v_2 = 1/3$ by using Eq. (35). It is observed that at $t = 0$ there is a stable equilibrium position. This is in agreement with that by Dundurs and Gangadharan [16] for a free-slipping interface. It is somewhat unexpected to see that, when $0 < t < 0.00473t_3^+$, there are two transient equilibrium positions for the dislocation: the one closer to the interface is an unstable one, whilst the other one further away from the interface is stable. The two equilibrium positions will merge to a single saddle point at $t = 0.00473t_3^+$. When $t > 0.00473t_3^+$, the dislocation will always be attracted to the inclusion.

The above calculations demonstrate that the dislocation mobility is rather complicated and the transient effect due to interface slip and diffusion cannot be neglected.

4.4. The interface diffusion occurs much faster than the interface slip ($\gamma \to 0$)

In this case, the relaxation times can be determined as

$$t_0 = t_n^- = 0, t_n^+ = \frac{\chi[n(\alpha+1)-2]}{2n(n-2)} = \frac{\chi}{2}\left[\frac{\alpha}{n-2} + \frac{1}{n}\right],$$
$$(n = 3, 4, \ldots, +\infty) \tag{37}$$

$A_n(t)$ and $B_n(t)$ can be obtained as

$$A_2(t) = 0,$$
$$A_n(t) = \frac{(n-2)[A_n(0) - \alpha B_n(0)]}{n(\alpha+1)-2} \exp\left(-\frac{t}{t_n^+}\right),$$
$$B_n(t) = \frac{n[\alpha B_n(0) - A_n(0)]}{n(\alpha+1)-2} \exp\left(-\frac{t}{t_n^+}\right), (n = 3, 4, \ldots, +\infty) \tag{38}$$

Similarly, it is found that $t_3^+ = \chi(3\alpha+1)/6$ is the longest time constant among the relaxation times $t_n^+ (n \geqslant 3)$. Thus, for the long-range stress relaxations one only needs to retain the terms $A_3(t)$ and $B_3(t)$ in the series expansions in Eqs. (10) and (19). The decaying internal stress field for long-range stress relaxations can thus be approximated as

$$\sigma_{xx} = \frac{2\beta\mu_2 b_y}{\pi\xi(\kappa_2+1)(\alpha-\beta-1)} + \frac{8\beta\mu_2 y[2R^2 b_y y + x(3\xi^2 - 2R^2)b_x]}{\pi R^2 \xi^3(\kappa_2+1)(3\alpha+1)} \exp\left(-\frac{t}{t_3^+}\right),$$
$$\sigma_{yy} = \frac{2\beta\mu_2 b_y}{\pi\xi(\kappa_2+1)(\alpha-\beta-1)} + \frac{8\beta\mu_2 x[-2R^2 b_y x + y(3\xi^2 - 2R^2)b_x]}{\pi R^2 \xi^3(\kappa_2+1)(3\alpha+1)} \exp\left(-\frac{t}{t_3^+}\right),$$

Table 1
Locations of the equilibrium position of the dislocation at different times ($\mu_1 = 10\mu_2$, $v_1 = v_2 = 1/3$ and $\chi \to 0$).

t/t_3^+	0.001	0.05	0.08	0.1	0.15	0.2	0.21	0.2128
ξ_0/R	1.0937	1.6575	1.9736	2.2275	3.2379	7.6598	16.6145	∞

Table 2
Locations of the equilibrium position of the dislocation at different times ($\mu_1 = 10\mu_2$, $\nu_1 = \nu_2 = 1/3$ and $\gamma \to 0$).

t/t_3^+	0	0.05	0.08	0.15	0.2	0.21	0.2128
ξ_0/R	2.4497	2.8549	3.1914	4.7265	10.584	22.7337	∞

$$\sigma_{xy} = \frac{4\beta\mu_2(2R^2 - 3\xi^2)(x^2+y^2)b_x}{\pi R^2\xi^3(\kappa_2+1)(3\alpha+1)}\exp\left(-\frac{t}{t_3^+}\right), (x^2+y^2<R^2) \tag{39}$$

By employing the Peach–Koehler formula, we arrive at an approximate but closed-form expression for the image force on the dislocation for long-range stress relaxations:

$$\begin{aligned}
F_x &= F_x^0 + \frac{2\beta\mu_2 R^2(b_y)^2}{\pi\xi^3(\kappa_2+1)(1-\alpha+\beta)} \\
&\quad + \frac{4\beta\mu_2 R^2[(\xi^2-2R^2)(3\xi^2-2R^2)(b_x)^2 + 4R^4(b_y)^2]}{\pi\xi^7(\kappa_2+1)(3\alpha+1)}\exp\left(-\frac{t}{t_3^+}\right), \\
F_y &= F_y^0 + \frac{2\beta\mu_2 R^2 b_x b_y}{\pi\xi^3(\kappa_2+1)(1-\alpha+\beta)} \\
&\quad - \frac{4\beta\mu_2 R^2(3\xi^2-4R^2)b_x b_y}{\pi\xi^5(\kappa_2+1)(3\alpha+1)}\exp\left(-\frac{t}{t_3^+}\right), |\xi| > R
\end{aligned} \tag{40}$$

If the dislocation is far from the inclusion and contains only the b_x component, then the glide force F_x can be obtained from Eq. (23) as

$$F_x = \frac{4\mu_2 R^2(b_x)^2}{\pi\xi^3(\kappa_2+1)}\left[\frac{3\beta}{3\alpha+1}\exp\left(-\frac{t}{t_3^+}\right) - 1\right], \quad \text{as } |\xi| \gg R \text{ and } t \geqslant 0 \tag{41}$$

Interestingly, the above expression is very similar to Eq. (35) except that the definitions of t_3^+ for the two cases are different. Therefore, the dislocation behavior, i.e. whether the dislocation is attracted to or repelled from the inclusion, is the same as that in Section 4.3.

In order to more clearly show the dislocation mobility due to its interaction with the inclusion, we illustrate in Fig. 4 the time-dependent glide force F_x on a dislocation containing only the b_x component for $\mu_1 = 10\mu_2$ and $\nu_1 = \nu_2 = 1/3$ by using the following exact solution:

$$\begin{aligned}
F_x &= -\frac{\mu_2(b_x)^2}{\pi(\kappa_2+1)}\frac{2R^2(2\xi^2-R^2)}{\xi^3(\xi^2-R^2)} + \frac{\beta\mu_2(b_x)^2}{\pi(\kappa_2+1)}\sum_{n=3}^{+\infty} \\
&\quad \times \frac{R^{2(n-2)}[(n-1)\xi^2-(n+1)R^2][n(n-1)\xi^2-(n+1)(n-2)R^2]}{\xi^{2n+1}[n(\alpha+1)-2]} \\
&\quad \times \exp\left(-\frac{t}{t_n^+}\right). \quad |\xi| > R \text{ and } t \geqslant 0
\end{aligned} \tag{42}$$

Again, the above series is truncated at $n = 50$ during the calculation. It is observed from Fig. 4 that when $0 \leqslant t < 0.2128t_3^+$ the dislocation has a transient unstable equilibrium position at $\xi = \xi_0$. At the initial moment, the equilibrium position is located at $\xi = 2.4497R$, which is at some distance from the interface. This situation is different from that observed in Fig. 2. As the time increases from $t = 0$ to $t = 0.2128t_3^+$, the equilibrium position will move outward from $\xi = 2.4497R$ to infinity (see Table 2). On the other hand, when $t > 0.2128t_3^+$, the dislocation will always be attracted to the inclusion. Our calculations also show that, for $t \geqslant t_3^+$, the approximate expression (40) for long-range stress relaxations can be used with very high accuracy.

4.5. The interface diffusion and slip have the same time scale $\chi = \gamma$ $(4\eta D = R^2)$

In this case, t_3^- and t_3^+ can be obtained as

$$t_3^- = \frac{\chi}{3}, \quad t_3^+ = \alpha\chi. \tag{43}$$

If the dislocation is far away from the inclusion and contains only the b_x component, then the glide force F_x can be obtained from Eq. (23) as

$$F_x = \frac{4\mu_2 R^2(b_x)^2}{\pi\xi^3(\kappa_2+1)}\left[\frac{\beta}{\alpha}\exp\left(-\frac{t}{t_3^+}\right) - 1\right], \text{ as } |\xi| \gg R \text{ and } t \geqslant 0 \tag{44}$$

Since we have assumed that the inclusion is stiffer than the matrix ($\beta > \alpha$), the dislocation will be attracted to or repelled from the inclusion depending on the time: (i) the dislocation will be repelled from the inclusion when $t < t_3^+ \ln(\beta/\alpha)$; (ii) the dislocation will be attracted to the inclusion when $t > t_3^+ \ln(\beta/\alpha)$.

5. Conclusions

We have obtained the time-dependent elastic field induced by a dislocation interacting with a circular inclusion with a rate-dependent imperfect interface on which slip and diffusion occur concurrently. The correctness of the obtained solution was verified by strict comparison with existing ones [7,15,16]. Thus our result is highly reliable. The far-field asymptotic expressions of the glide and climb forces on the dislocation were obtained in Eqs. (23) and (24). The dislocation mobility due to its interaction with the inclusion was discussed by considering five extreme cases of the interface. Our discussions in Section 4 clearly show that, under certain conditions, the dislocation will be repelled from the inclusion for an initial period of time and then be attracted to the inclusion as a result of the stress relaxation by interface slip and diffusion. Our calculations in Sections 4.3 and 4.4 demonstrate that the transient effect due to interface slip and diffusion cannot be ignored if one wants to know the intricate details of the dislocation–inclusion interaction.

Finally it is interesting and challenging to consider the transient response induced by a straight dislocation interacting with a spherical inclusion with simultaneous interface slip and diffusion. While the corresponding steady-state response was discussed in some detail by Gao [17], the corresponding transient stress relaxation without dislocation was presented by He and Hu [18]. It is expected that the time scaling of the slip and diffusional relaxations in the three-dimensional case will be different than that in the two-dimensional case [7].

Acknowledgement

This work was supported by the Bairen Program in Henan Province.

References

[1] Raj R, Ashby MF. Metall Trans 1971;2:1113.
[2] Herring C. In: Kingston WE, editor. The physics of powder metallurgy. New York: McGraw-Hill; 1951. p. 143.
[3] Koeller RC, Raj R. Acta Metall 1978;26:1551.
[4] Srolovitz DJ, Petkovic-Luton R, Luton MJ. Scripta Metall 1982;16:1401.
[5] Srolovitz DJ, Petkovic-Luton R, Luton MJ. Philos Mag 1983;48:795.
[6] Srolovitz DJ, Petkovic-Luton R, Luton MJ. Acta Metall 1983;31:2151.
[7] Srolovitz DJ, Luton MJ, Petkovic-Luton R, Barnett DM, Nix WD. Acta Metall 1984;32:1079.
[8] Mishin Y, Asta M, Li J. Acta Mater 2010;58:1117.
[9] Mishra RS. JOM 2009;61:52.
[10] Wei YJ, Bower AF, Gao HJ. J Mech Phys Solids 2008;56:1460.
[11] Muskhelishvili NI. Some basic problems of the mathematical theory of elasticity. Groningen: Noordhoff; 1953.
[12] Sofronis P, McMeeking RM. Mech Mater 1994;18:55.
[13] Wang X, Pan E. Int J Eng Sci, in press.
[14] Peach MD, Koehler JS. Phys Rev 1950;80:436.
[15] Dundurs J, Mura T. J Mech Phys Solids 1964;12:177.
[16] Dundurs J, Gangadharan AC. J Mech Phys Solids 1969;17:459.
[17] Gao HJ. Int J Eng Sci 1992;30:1061.
[18] He LH, Hu XF. Mater Chem Phys 2002;77:147.